

Interplay of RhoA and mechanical forces in collective cell migration driven by leader cells

M. Reffay^{1,2}, M. C. Parrini³, O. Cochet-Escartin¹, B. Ladoux^{2,4}, A. Buguin¹, S. Coscoy¹, F. Amblard¹, J. Camonis^{3,5} and P. Silberzan^{1,5}

The leading front of a collectively migrating epithelium often destabilizes into multicellular migration fingers where a cell initially similar to the others becomes a leader cell while its neighbours do not alter. The determinants of these leader cells include mechanical and biochemical cues, often under the control of small GTPases. However, an accurate dynamic cartography of both mechanical and biochemical activities remains to be established. Here, by mapping the mechanical traction forces exerted on the surface by MDCK migration fingers, we show that these structures are mechanical global entities with the leader cells exerting a large traction force. Moreover, the spatial distribution of RhoA differential activity at the basal plane strikingly mirrors this force cartography. We propose that RhoA controls the development of these fingers through mechanical cues: the leader cell drags the structure and the peripheral pluricellular acto-myosin cable prevents the initiation of new leader cells.

When cells of an epithelium are presented *in vitro* with a free surface—created, for example, by a wound¹ or by the release of a physical barrier²—they migrate collectively while still maintaining strong cell–cell adhesions. This collective migration^{3,4}, characterized by coordinated long-range displacements within the monolayer, often coexists with a strong fingering of the leading edge where the pluricellular migration fingers are preceded by leader cells^{2,5,6}. Interestingly, similar structures are also observed *in vivo* in diverse situations such as morphogenesis¹ or cancer invasion^{7,8}.

At the start of migration, a cell initially similar to the others changes its phenotype into a ‘leader cell’. Its neighbours at the border do not undergo this transformation, and thus long migration fingers develop. The initiation of the leader cell is determined by mechanical cues resulting from, and acting on, intracellular biochemical activities^{9,10}. Of particular interest in this context is the distribution of the mechanical traction forces within these fingers and at the leader cell, and the coordination of these forces and the local biochemical activity of GTPases such as RhoA and Rac1. In contrast to single-cell migration, the mechanics of collective migration has been investigated only in the past few years^{11–14}. Similarly, the roles of RhoA and Rac1—whose importance in single-cell motility^{15,16} and in cell mechanics¹⁷ has long been recognized—have only recently been explored in more collective processes such as embryogenesis-related

collective migration^{18,19}, invasion from tumours²⁰ and wound-healing assays^{9,21}.

In this study, we directly investigated the correlation between GTPase activity and the mechanical forces in migration fingers by mapping in parallel the traction forces developed on the surface by the cells that constitute these structures and the local activity of RhoA and Rac1 in these cells. The experiments were conducted with epithelial Madin–Darby canine kidney (MDCK) cells using the ‘model wound assay’, in which cells are cultured in the apertures of micro-stencils. Peeling off these stencils triggers migration and finger formation without damaging the cells² (Supplementary Fig. 1A, B). Forces were then dynamically mapped using a dense array of soft micro-pillars as the underlying substrate, with each pillar acting as an independent force sensor²². The local activities of RhoA and Rac1 were measured at the basal plane of live cells transfected with the appropriate fluorescence resonance energy transfer (FRET)-based biosensor²³.

RESULTS

Migration fingers are mechanical global entities

As previously reported², fingers began to form two hours after the start of the experiments. Traction forces were measured in well-formed, long, mature structures (length d_0 , $40 \mu\text{m} < d_0 < 100 \mu\text{m}$,

¹Laboratoire Physico-chimie Curie—UMR 168, Institut Curie, Centre de Recherche, CNRS, UPMC, Paris, F-75248, France. ²Laboratoire Matière et Systèmes Complexes—UMR 7057, Université Paris Diderot, CNRS, Paris, F-75251, France. ³Analysis of Transduction Pathways Group—U830, Institut Curie, Centre de Recherche, Inserm, Paris, F-75248, France. ⁴Present address: Institut Jacques Monod (IJM), CNRS UMR 7592 & Université Paris Diderot, Paris F75205, France and Mechanobiology Institute, National University of Singapore 117411, Singapore.

⁵Correspondence should be addressed to J.C. or P.S. (e-mail: jacques.camonis@curie.fr or pascal.silberzan@curie.fr)

Received 15 March 2013; accepted 10 January 2014; published online 23 February 2014; DOI: 10.1038/ncb2917; corrected online 26 February 2014

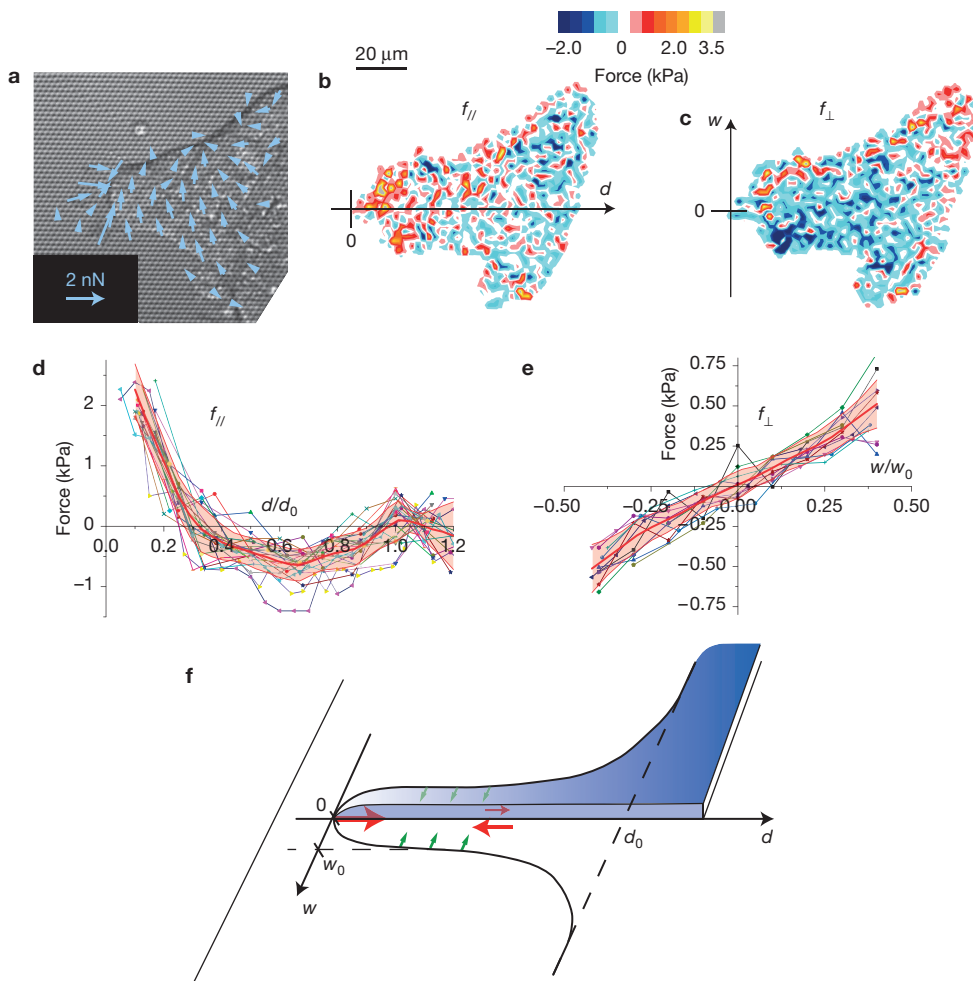


Figure 1 Traction forces exerted on the surface by the migration fingers. **(a–c)** Mapping of the traction forces obtained by the micro-pillar technique **(a)** and intensity of the projected component in the longitudinal **(b)** and transverse **(c)** directions. Only a fraction of the forces has been represented in **a** for clarity (representative images, replicated more than 20 times). **(d,e)** Force profiles in the parallel and perpendicular directions resulting from averaging forces for 22 and 12 fingers from 15 and 10 independent experiments respectively. The thick red line is the average profile, the coloured area represents the standard deviation. **(f)** Schematic representation of the direction of the forces: the leader cell exerts a stable traction longitudinal force whereas the forces in the fingers are highly dynamic and can be positive or negative (red arrows). The side edges exert a centripetal force (green arrows). Fingers were composed of typically 30 cells.

Fig. 1a) and were decomposed into two orthogonal components: parallel (longitudinal; f_{\parallel}) and perpendicular (transverse; f_{\perp}) to the finger axis (Fig. 1b,c).

In Fig. 1d,e the longitudinal and transverse force profiles obtained through the analysis of these maps were renormalized by the fingers' length (d_0) and width (w_0), respectively. The longitudinal force f_{\parallel} (Fig. 1d) at the tip was very large and positive (that is, directed from the tip of the finger towards its base (Fig. 1f)) but became negative within a couple of cell rows. The large pulling traction forces exerted by the leader cell could locally reach more than 2 kPa corresponding to a total integrated force of 40 nN under the lamella, where actin co-localizes with the phosphorylated active form of myosin²⁴ (Fig. 2a–c). These forces were greater than the average value measured at the edge of a growing epithelium on a low-rigidity substrate¹². Within the fingers, traction forces were highly dynamic and mostly localized at the cell–cell junctions²². They could locally be positive or negative, meaning that the cells forming

these structures move actively within them^{14,25}. When averaged out, f_{\parallel} was negative for $0.3 \cdot d_0 < d < d_0$, corresponding to an effective friction, with a minimum for $d \approx 0.7 \cdot d_0$ (Fig. 1d). Remarkably, as classically observed in single cells²⁶, the measured forces were proportional to the effective substrate rigidity in the 1–20 kPa range (Supplementary Fig. 1C,D).

The forces f_{\perp} perpendicular to the finger direction were greatest at the two borders and overall directed towards its centre, so that both sides of the fingers were, on average, balanced (Fig. 1e). They did not show significant variations along the finger principal direction and were lower than the maximal longitudinal forces (up to ~1 kPa; Fig. 1e). The spatial distribution of the observed forces in the fingers is summarized in Fig. 1f.

The distribution of forces at the tissue scale is reminiscent of migrating single cells such as fibroblasts²⁷ or keratocytes^{28,29}, meaning that the finger progresses on the surface as a global mechanical entity in which forces are transmitted from cell to cell to produce

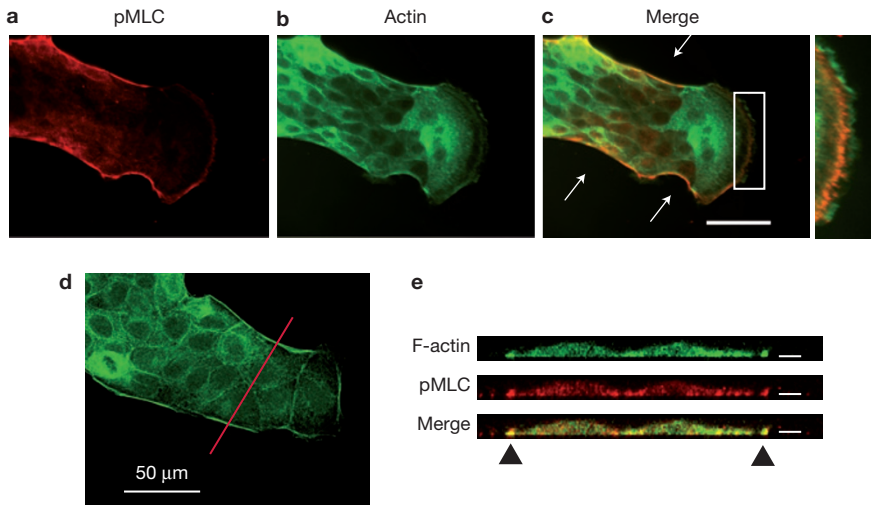


Figure 2 Presence of pluricellular acto-myosin structures at the fingers. **(a–c)** Phosphorylated myosin light chain (pMLC; immunofluorescence micrograph, **a**) and GFP-actin (**b**) co-localize at the scale of the finger in the form of a pluricellular acto-myosin cable (arrows) and at the leader lamella (**c**; zoom).

Scale bar: 50 μm . **(d,e)** Confocal section of a fixed finger showing the co-localization of F-actin and pMLC in the basal plane at the cable (triangles). The red line depicts the section plane. Scale bars of the x-z sections: 5 μm . (Representative images, 5 replicates.)

a coordinated motion^{12,14}. This directly confirms the concept of a mechanically self-consistent ‘super-cell’ as originally proposed in ref. 10.

The distribution of the transverse forces could be related to the presence of a pluricellular tensile acto-myosin cable along the edges of the finger and that localizes at the basal side of the structure^{9,30} (Fig. 2a–e). Indeed, when this cable was cut by photoablation-induced nanosurgery, it retracted in typically 30 s (Fig. 3a and Supplementary Fig. 2A,B and Supplementary Movie 1). Severing the cable also induced the displacement of nearby intracellular structures and triggered the relaxation of pillars along the cable but not directly at the cut (Fig. 3a and Supplementary Fig. 2C). Therefore, the actin cable is under tension³¹ similar to what is observed at the dorsal closure of the *Drosophila* embryo³², and interacts directly with the underlying substrate.

Furthermore, severing the cable led to the nucleation of a new leader cell at the precise location of the cut in a large fraction (~60%) of the experiments ($n=22$; Fig. 3b and Supplementary Movie 2). An analysis of the velocity field within these newly formed structures unambiguously identified them as migration fingers (Fig. 3c). In the absence of external perturbation, new fingers also spontaneously initiated at ‘weak points’ in the cable as characterized by their lower green fluorescent protein (GFP)-actin fluorescence, as they developed their characteristic force profile (16 positive observations on 17 nascent fingers in 3 different experiments; Supplementary Fig. 3A). These data point to a ‘confining’ role for the acto-myosin cable, whose stored tension mechanically prevents the initiation of new leader cells and therefore allows the development of long fingers.

GTPases activities are distributed along the fingers

We also assessed GTPase activity during collective migration through the use of specific inhibitors: Y27632, which inhibits the action of ROCK downstream of Rho; blebbistatin, which targets the action of the myosins; and C3 transferase, which acts directly on Rho.

None of these inhibitors prevented migration but they all inhibited the formation of well-formed fingers, as did short interfering RNAs (siRNAs) targeting RhoA (Fig. 4a and Supplementary Fig. 4A–B), which is in agreement with previously reported results^{5,25}. Moreover, when these drugs were added after the fingers had formed, the traction force profile changed markedly (Fig. 4b,c). In particular, when using Y27632, the force at the leader cell became clearly negative (Fig. 4b), indicating that the leader cell had switched from pulling its followers to being pushed by them. In contrast, the Rac GEF inhibitor NSC 23766 had very limited influence on the migration of the monolayer (the average velocity and morphology of the border remained the same; Fig. 4a and Supplementary Fig. 4A), suggesting that Rac1 activation is not crucial in this process. We therefore conclude that the mechanism underlying finger development is mainly under RhoA control.

By analysing motile MDCK cells expressing the FRET biosensor Raichu-RhoA (RhoACter) or Raichu-Rac1 (Rac1Cter), we could dynamically map the activity of these GTPases within the fingers. Here, we took advantage of the relatively low transfection efficiency (typically 5% of the cells) to image individual fluorescent cells within a majority of ones that were not fluorescent. The flat and extended lamellipodia of the leaders in which cyan fluorescent protein (CFP) intensity was too low were excluded from the analysis. Raichus are sensors of the presence of GEF activity (or of a positive GEF/GAP balance), not of RhoA or Rac1 localization nor of endogenous GTP-bound RhoA or Rac1. A limitation is that Raichus cannot completely reflect the physiological RhoA or Rac1 localization for various reasons, including their incapacity to bind to guanosine nucleotide dissociation inhibitors, which play an important role in the cytosol-membrane shuttling of Rho GTPases. Nevertheless, it is commonly accepted that a positive GEF/GAP balance detected by Raichus mirrors an increased activity of endogenous RhoA or Rac1 (ref. 33).

Live FRET confocal microscopy about the basal plane showed that RhoA activity primarily localizes within 2 μm of the plane

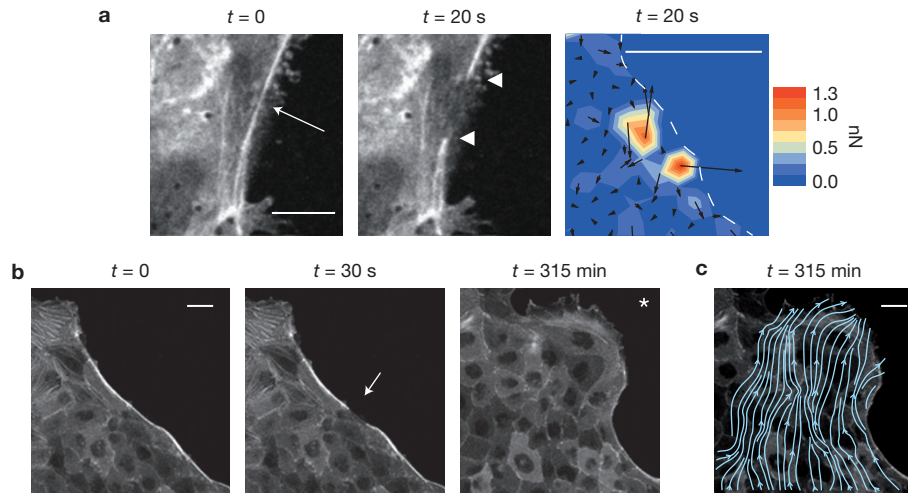


Figure 3 The contractile acto-myosin cable controls the initiation of new leader cells. **(a)** When cut by laser photoablation (arrow), the cable retracts rapidly (the extremities of the severed cable are denoted by the two triangles after 20 s; see also Supplementary Fig. 2A,B), which indicates that it is under tension. GFP–actin, scale bar, 10 μ m. This retraction is accompanied by local traction forces on the surface demonstrating the strong coupling of this cable to the substrate (Supplementary Fig. 2C). Representative images of > 20 replicates. **(b)** The ablation of the cable triggers the appearance of a new leader cell, demonstrating its ‘confinement’ function in preventing the

onset of new leaders. The arrow shows the point of laser ablation, and the asterisk is next to the new leader cell that starts to develop at this ablation point on the cable. GFP–actin, scale bar, 20 μ m. **(c)** The flow lines that show the direction of displacements were obtained from the mapping of the whole displacement field by particle image velocimetry as described in ref. 2. Each flow line is tangent to the local velocity at any point. Their high directionality over the whole finger that extends within the epithelium unambiguously identifies these structures as migration fingers (see Supplementary Movie 2). Representative images of 20 replicates.

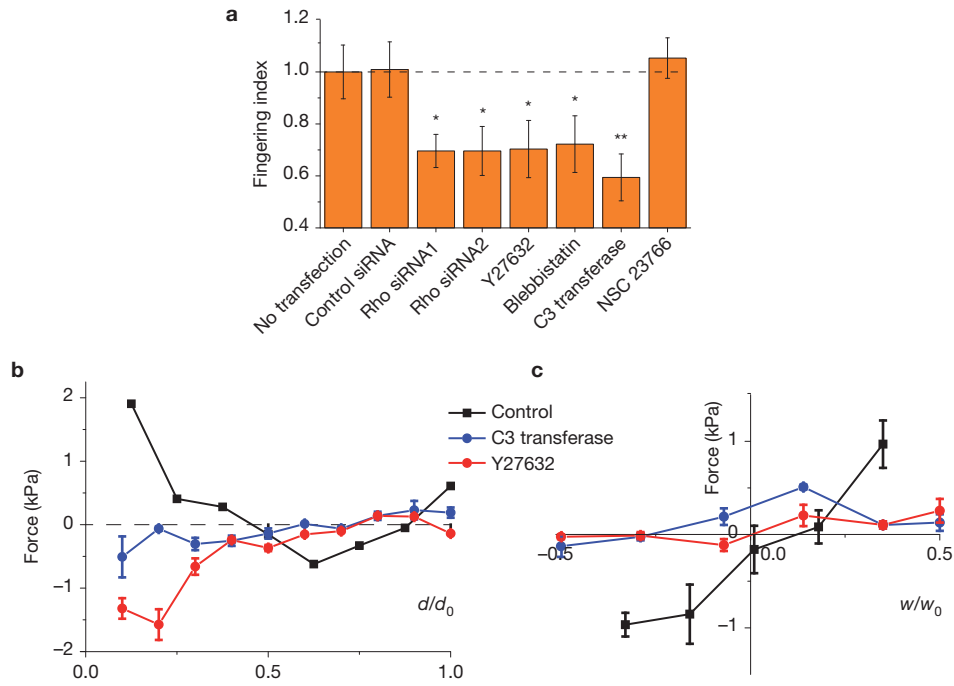


Figure 4 The force profiles under the fingers are under RhoA control. **(a)** Fingering index (root mean square distance between the actual profile and the line figuring its average position). Fingering index values have been normalized to the control value. Inhibitors against RhoA as well as siRNAs directed against RhoA show a significant decrease of the fingering index whereas the Rac1 inhibitor does not (see also Supplementary Fig. 4). Each bar results from averaging 6 distinct experiments. Error bars are s.e.m. (* $P < 0.05$; ** $P < 0.001$. Two-sample t -test). **(b,c)** Evolution of the traction forces developed by well-formed fingers following the addition of RhoA

inhibitors. Forces were measured 30 min to 2 h after addition of the inhibitor. **(b)** Longitudinal forces: a decrease (C3 transferase) and even an inversion (Y27632) of the force profile is seen following the addition of Rho inhibitors to a well-established finger. The phenotype close to the tip ($d/d_0 < 0.2$) switches from pulling the followers (positive forces) for the control, to being ‘pushed’ by them when Rho is inhibited by Y27632 (negative forces). $n = 3$ fingers from 2 independent experiments. Error bars are s.e.m. **(c)** The transverse forces sharply decrease to very small values following the addition of the inhibitors. $n = 3$ fingers from 2 independent experiments. Error bars are s.e.m.

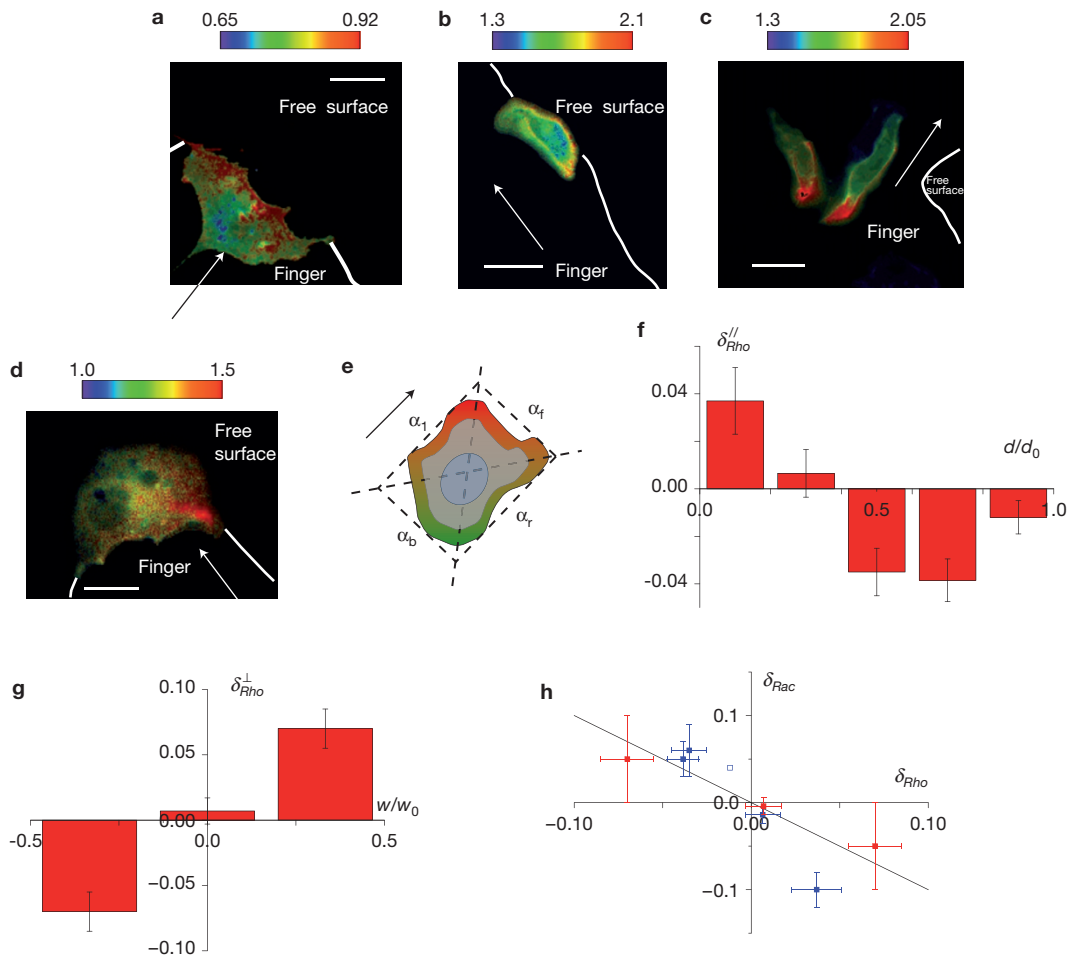


Figure 5 Mapping of RhoA and Rac1 differential activities within migration fingers. **(a–c)** Examples of the distribution of RhoA activity at the basal plane at several locations within a finger. For a leader cell, RhoA activity is highest at the front edge **(a)**. The distribution is inverted for cells closer to the epithelium **(c)**. Cells next to the acto-myosin cable have increased RhoA activity on the side adjacent to this cable **(b)**. The arrow is parallel to the finger axis and points towards the leader cell. **(d)** Rac1 differential activity at the leader cell. Note the decreased activity at the front of the leader cell compared with its rear (note that the cell immediately behind is not labelled). As for RhoA analysis, the low-fluorescence flat lamellipodium is excluded from the FRET analysis. Scale bars, 10 μm . (Representative images in **a, d**: 3 replicates; **b,c**: more than 20 replicates). **(e)** Definition of the differential activity. The arrow denotes the direction of migration of the cell. The activities α_x at the front, back, left and right are defined by the quadrants of the rectangle parallel to the direction of migration (arrow).

for the finger cells and at the top of the lamella for the leader cells (Supplementary Fig. 5). FRET confocal and non-confocal wide-field microscopies gave similar results (Fig. 5a–c and Supplementary Fig. 5): on the sides of the fingers, RhoA activity co-localized with the actin cable as previously mentioned (Fig. 5b and Supplementary Fig. 5B); and at the front side of the leader cells, most of the activity localized at the lamella²⁴ (Fig. 5a and Supplementary Fig. 5A), where we independently observed a high concentration of phospho-myosin light chain (Fig. 2c). Farther away from the tip of the finger, the activity was more localized at the cell rear-side (Fig. 5c and Supplementary Fig. 5C).

These quantities are used in the calculation of the differential activities as defined in the text. To exclude the spurious activity next to the nucleus, only the region next to the cell border is taken into account (width 0.6 μm). **(f)** Evolution of the longitudinal Rho differential activity along an ‘average finger’ obtained by binning and averaging ($n=30$ cells from 7 independent experiments). Error bars are s.e.m. **(g)** Transverse differential activity of Rho across the finger ($n=20$ cells from 5 independent experiments). Error bars are s.e.m. Note the same evolution as the corresponding force (Fig. 1d,e). **(h)** Relationship between the differential activities of RhoA and Rac1 for cells identically positioned within a finger in normalized coordinates. Blue points: longitudinal activities; red points: transverse activities. The line has a slope (-1) and illustrates the anticorrelation between these two quantities. $n=42$ cells from 10 independent experiments for Rho activity measurements, $n=20$ cells from 5 experiments for Rac activity measurements. Error bars are s.e.m.

To compare these results with the observed mechanical forces requires the activity gradient of the GTPases to be quantified at the cellular scale. Consequently, we defined the cells’ differential activities along the direction of the finger as³⁴: $\delta_{GP}^{||} = (\alpha_{GP}^f - \alpha_{GP}^b)/(\alpha_{GP}^f + \alpha_{GP}^b)$, where α_{GP}^x denotes the local subcellular activity of the G protein of interest (that is, RhoA or Rac1) at the cell front ($x=f$) and back ($x=b$) (Fig. 5e). Similar expressions were derived for δ_{GP}^{\perp} for the left-right activities. This last quantity was symmetrized about the finger axis. Rac1 and RhoA differential activities were a function of the position of the cells within the fingers (Fig. 5f,g and Supplementary Movies 3–5).

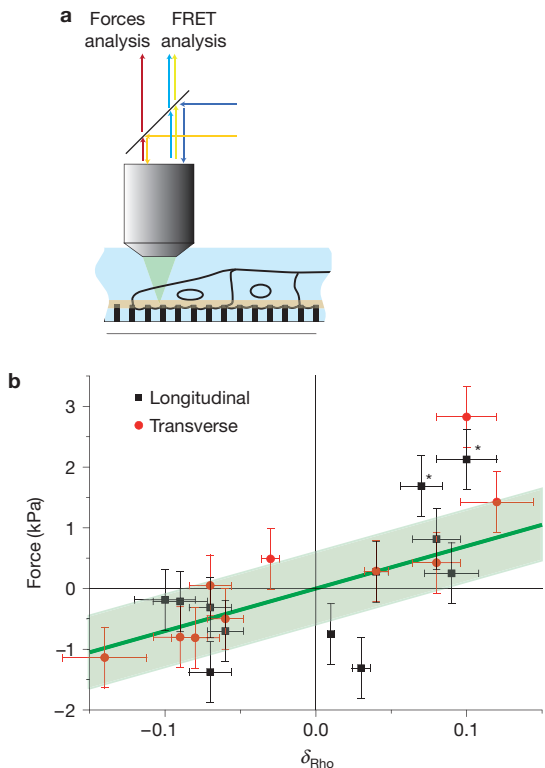


Figure 6 Traction forces and Rho differential activity are directly correlated. (a) Experimental set-up that allows the traction forces (red channel) and the FRET signal (yellow and cyan channels) to be measured on the same cells. Both signals were successively co-registered at the basal plane (orange slice) with an upright confocal microscope. (b) The total force developed by a given cell plotted against the corresponding differential activity (one point corresponds to one cell). δ_{Rho} and the force are of the same sign and proportional to each other. The same trend is confirmed on an averaged finger by accumulating data collected on independent fingers (Supplementary Fig. 6). The asterisks indicate leader cells. Error bars are experimental uncertainties. $n=12$ cells from 3 independent experiments.

Interestingly, by comparing cells located at the same normalized position, we found that δ_{Rho} and δ_{Rac} were quantitatively exactly anticorrelated in both directions within the limits of our experimental precision (Fig. 5h).

At the front edge of the leader cell body, we observed high levels of RhoA activity (Fig. 5a) and low Rac1 activity (Fig. 5d). These distributions complement the previously reported enhancement of the activities of these proteins at the leading edge of the lamellipodium^{16,33,35,36}, which we did not include in our analysis because of low expression levels of the biosensors. Our data thus highlight again the central role of the leader cell's lamella that seems to be under RhoA control³⁶. The transverse distribution of RhoA activity is maximum at the edges of the fingers, which reflects the co-localization of this GTPase with the acto-myosin cable³⁷.

Notably, leader cells are clearly not predetermined by an intrinsic RhoA polarity. When still in the monolayer, cells that eventually become leaders are initially characterized by a close-to-zero $\delta_{\text{Rho}}^{||}$. As the finger forms and the phenotype of these cells changes to that of a leader, the gradient of Rho activity across the cell and the global force distribution both develop in parallel over a timescale of a few hours (Supplementary Fig. 3B,C). The formation and maintenance of these migration fingers therefore involve different roles for RhoA (ref. 21).

The supracellular distribution of RhoA activity mirrors the cartography of forces

When plotted against the normalized finger length or width, δ_{Rho} showed the same spatial variations as the mechanical forces that we measured and, in particular, the same sign change (Fig. 5f versus 1d, Fig. 5g versus Fig. 1e). Confocal observations performed directly on the fingers progressing on the micro-pillars showed a spatial localization of the RhoA FRET signal close to the basal plane where the traction forces are exerted (Fig. 6a and Supplementary Fig. 5). Moreover, inhibiting RhoA with C3 transferase resulted in a marked decrease in RhoA differential activity all along the finger, which mirrors the decrease in the force profile under similar conditions (Fig. 4b and Supplementary Fig. 4C). We therefore conclude that there is a strong direct correlation between Rho activity and the traction forces.

Indeed, there is a clear relationship between these quantities as shown in Fig. 6b, in which we plot the force developed by a given cell within the finger versus its RhoA differential activity measured in the plane corresponding to the top of the pillars. The traction forces were proportional to RhoA differential activity with a sensitivity (that is, the proportionality constant) of 7 ± 2 kPa (Fig. 6b). Concatenating data obtained by wide-field fluorescence microscopy on an 'average finger' confirmed that δ_{Rho} is proportional to the generated force with the same sensitivity as the confocal direct measurements (Supplementary Fig. 6).

DISCUSSION

Taking all these data together, we have shown that the fingers behave as mechanical global entities, with the leader cell dragging its followers by the large force it develops. The transmission of the forces within the structure establishes a tissue-scale coherent force profile and sets the peripheral actin cable under tension. Moreover, this supracellular mechanical organization corresponds to local gradients of RhoA activity at the level of the individual cells that constitute the finger. The striking correlation between the differential activity of RhoA and the local force clearly shows that this particular protein controls the migration fingers through active contractility. This relationship between tension, actin superstructures and Rho activation is yet another example of the transposition of concepts that have been validated on single cells³⁸ to the multicellular scale.

The importance of pluricellular peripheral acto-myosin contractile structures for the cohesion of pluricellular clusters has been underlined in two- and three-dimensional environments^{21,39}. By analogy, we propose that the cable discussed in the present study mechanically prevents the initiation of new leader cells within an already formed finger and therefore ensures the development of long migration fingers. The co-localization of RhoA activity with the cable illustrates again the strong correlation between this protein and mechanical forces. Previous observations have convincingly demonstrated the activation of RhoA by mechanical tension^{40,41}. We reason that this locally increased RhoA activity may in turn act positively on the contractility of the cable. Therefore, the force exerted by the leader cell on the whole structure induces a mechanical positive feedback loop on the cable tension through Rho activation. By this mechanism, a pluricellular coherent structure thus emerges, based on the spatial distribution of Rho activity at the level of single cells.

was excluded from the FRET analysis. Forty-two cells in 10 independent experiments were studied for RhoA activity and 20 cells in 5 independent experiments for Rac1.

In Fig. 6b, forces and differential activities were measured simultaneously. In the other cases, quantitative comparisons of differential activities and forces were performed in parallel on cells identically localized within a finger after its normalization by its total length and total width. For better statistics, the values

were averaged in bins (typically 5 bins along the length and 3 bins across the width). At least 5 cells were counted in each bin.

When indicated, flow lines were calculated from the velocity field measured by particle image velocimetry⁵⁰ as described in ref. 51. These flow lines locally tangent the velocity at every point.

Unless otherwise noted, the error bars indicate the standard error of the mean (s.e.m.).

Interplay of RhoA and mechanical forces in collective cell migration driven by leader cells

M. Reay, M. C. Parrini, O. Cochet-Escartin, B. Ladoux, A. Buguin, S. Coscoy, F. Amblard, J. Camonis and P. Silberzan

Nat. Cell Biol. **16**, 217–223 (2014); published online 23 February 2014; corrected after print 26 February 2014

In the version of this Article originally published there were some errors:

The second citation of reference 1 in the first sentence of the main text should have been of reference 2 ('...or by the release of a physical barrier²...').

The present addresses of B. Ladoux were missing the area codes ('Paris F75205' and '117411 Singapore').

The caption of Fig. 1d–f should have read: '(d,e) Force profiles in the parallel and perpendicular directions resulting from averaging forces for 22 and 12 fingers from 15 and 10 independent experiments respectively. The thick red line is the average profile, the coloured area represents the standard deviation. (f) Schematic representation of the direction of the forces: the leader cell exerts a stable traction longitudinal force whereas the forces in the fingers are highly dynamic and can be positive or negative (red arrows). The side edges exert a centripetal force (green arrows). Fingers were composed of typically 30 cells.'

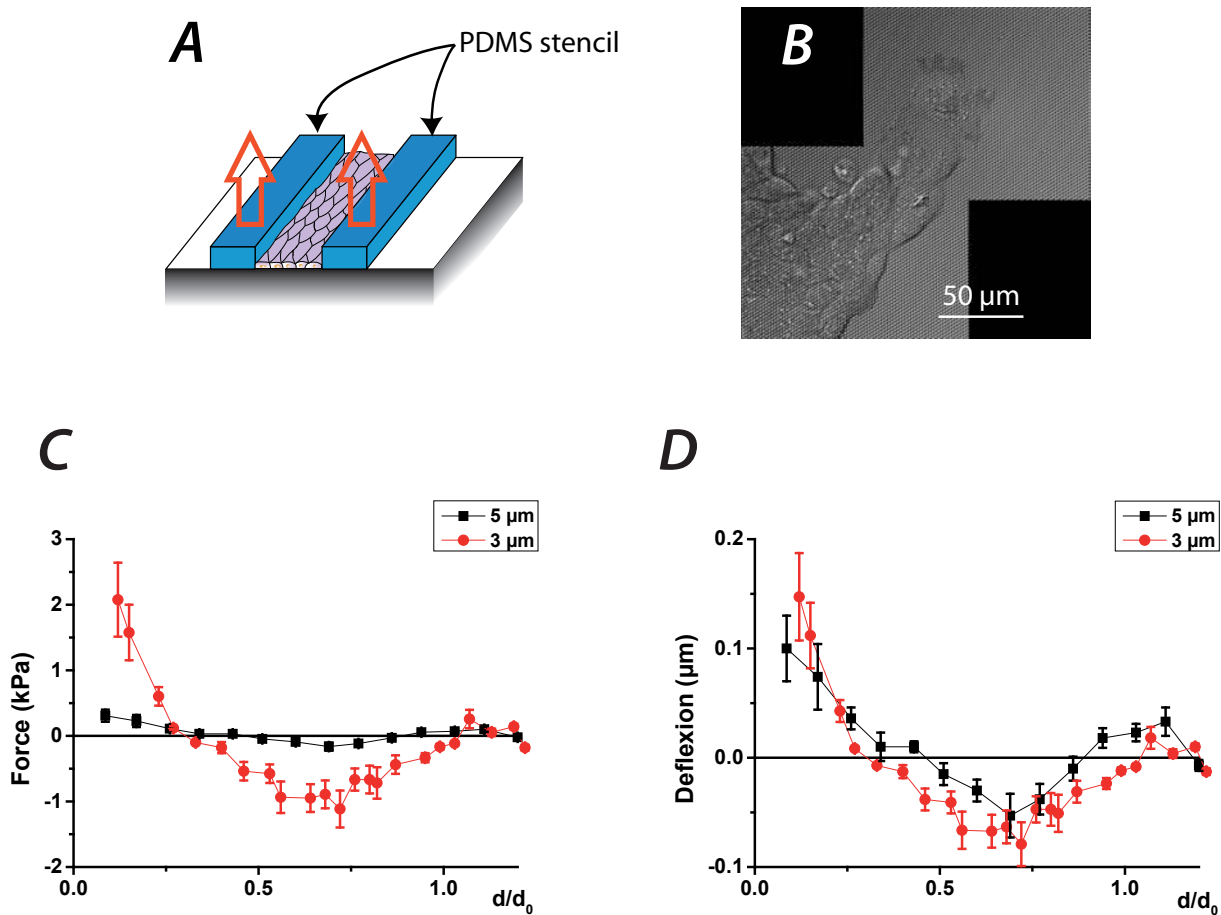
In the first sentence of the second paragraph under the heading 'Migration fingers are mechanical global entities', the figure citation should have read 'Fig. 1d,e'.

The first part of the caption of Fig. 3c should have read: '(c) The flow lines that show the direction...'

The citation of 'Supplementary Fig. 4C,B' in the first paragraph under the heading 'The supracellular distribution of RhoA activity mirrors the cartography of forces' should have read 'Fig. 4b and Supplementary Fig. 4C'.

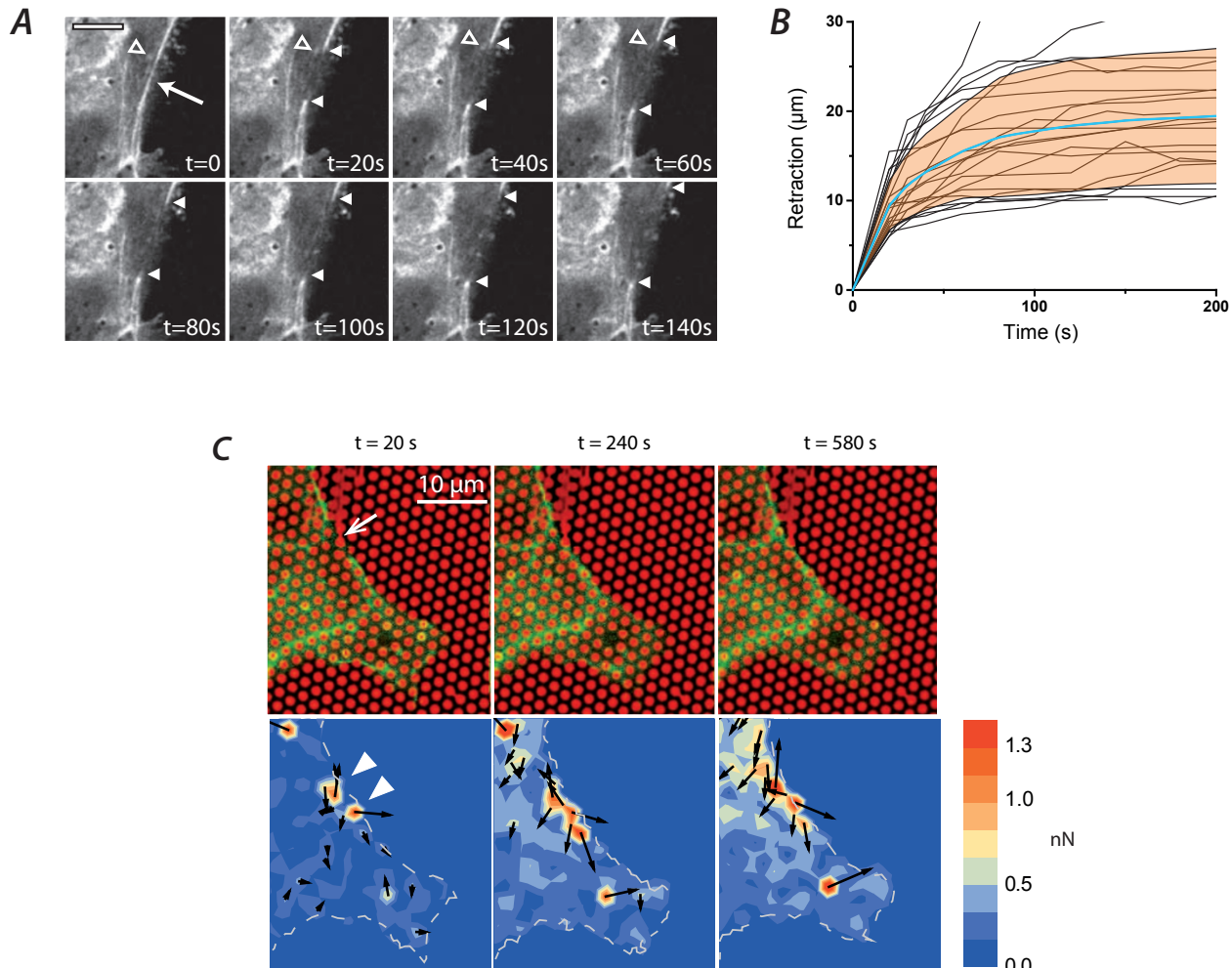
The page ranges for refs 17, 28, 44, 46 were missing; they are 15895–15900, 1313–1323, 6582–6591 and 1836–1843, respectively.

All these errors have been corrected in the online versions of the Article.



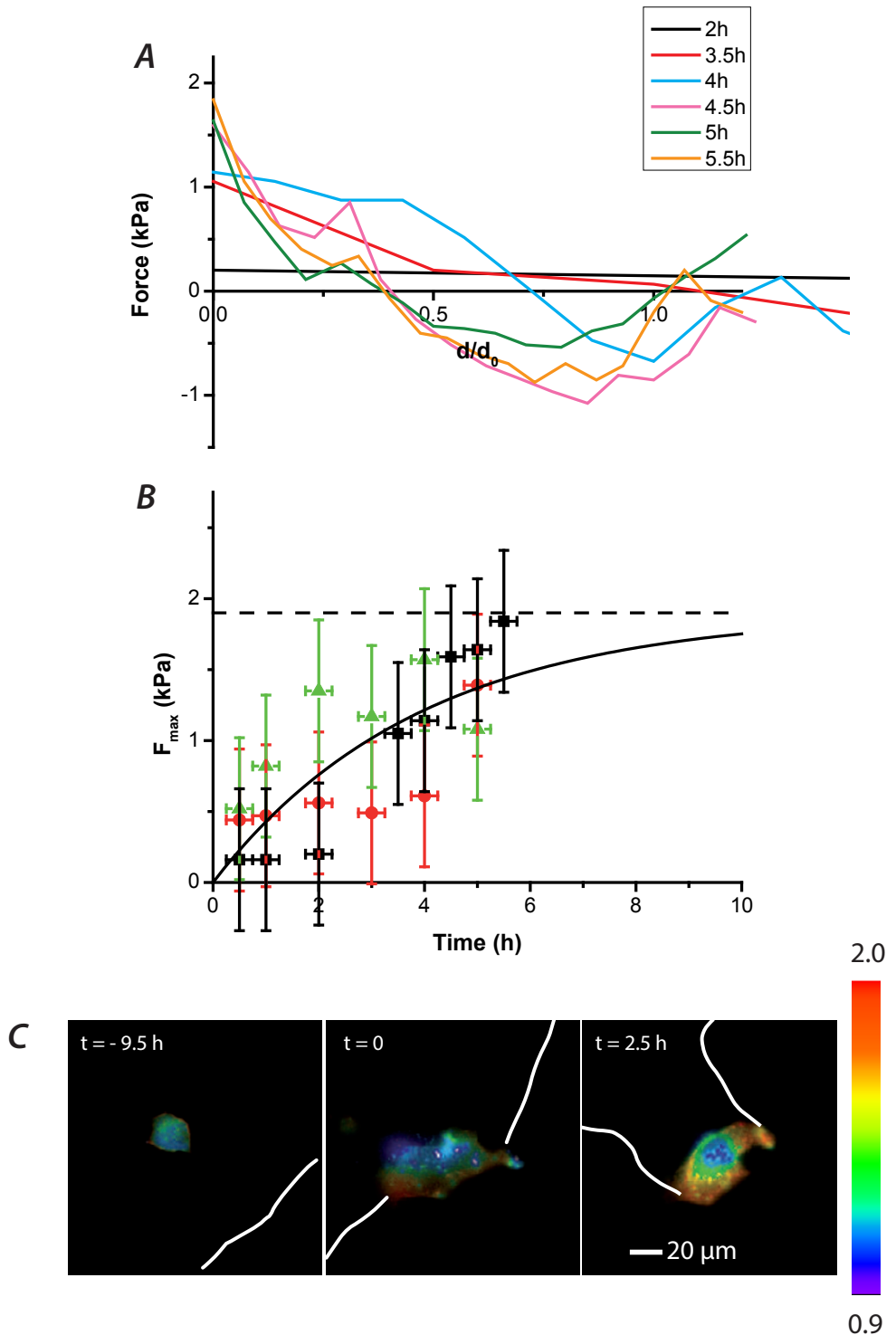
Supplementary Figure 1 Migration fingers respond to the micropillar array rigidity. (A) Experimental set-up. The microstencil is deposited on the surface; cells are then seeded and cultured until confluence in the apertures. Peeling off the stencil triggers cell migration on the free surface. (B) Fingers develop well on a micropillar array. Phase contrast image of the migrating front on a micropillar array. The fingers are clearly identified. They are preceded by a leader cell of a specific phenotype. Representative image, more than 20 replicates. (C–D) Influence of the substrate rigidity on the force profile. (C)

Forces were measured on substrates differing on the height of the pillars and hence on their effective rigidity (see Material and Methods). The absolute forces were very different. (D) In contrast, the deflection of the pillars does not depend on their rigidity (i.e. the forces are proportional to the surface rigidity). 5 μm high pillars correspond to an effective Young Modulus of 1.7 kPa; 3 μm high pillars correspond to an effective Young modulus of 7.8 kPa¹. 5μm-pillars: n = 10 fingers from 3 independent experiments; 3μm-pillars: n = 9 fingers from 3 independent experiments. Error bars are SEMs.



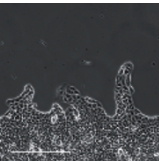
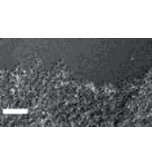
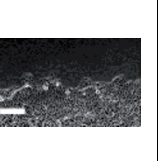
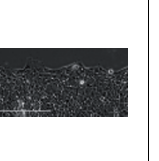
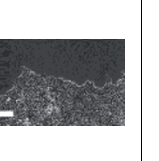
Supplementary Figure 2 The peripheral actin cable is under tension and interacts directly with the substrate (**A**) Image sequence following the severing of the actin-GFP cable by photoablation (scale bar 10 μm). The white arrow indicates the initial ablation. The solid triangles denote the extremities of the retracting cable (see also Supp. Movie 1). Note that small structures next to the cable retract as well (empty triangle), demonstrating that this is a tension driven relaxation. Representative images. More than 20 replicates. (**B**) Distance between the two extremities of the cable as a function of time. The cyan line is the average of the different independent measurements (black curves), yielding a characteristic time of 37 ± 7 s

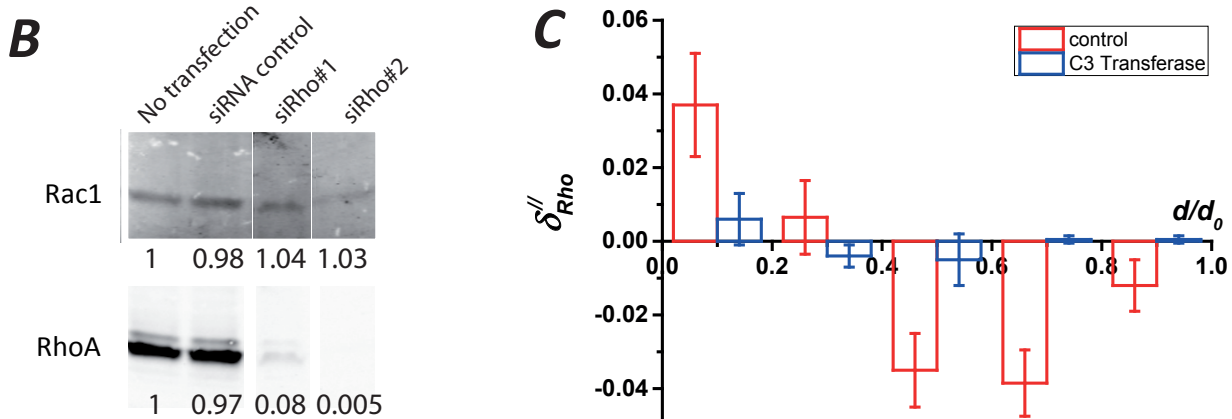
(SD) after a fit by an exponential function. The orange area is the standard deviation over 20 experiments. (**C**) When cut by photoablation (top panel, arrow), not only the forces at the cut relax but also the neighboring pillars situated under the cable. $t=0$ is the time of ablation. Top panel = actin-GFP and pillars – bottom panel = local forces (colours give the intensity and arrows the direction). The white triangles denote the high forces at pillars next to the cut. Note that the relaxation at longer times involves more pillars at a distance from the physical cut which demonstrates the direct interaction of the tensile actin cable with the substrate. Representative image. 20 replicates.



Supplementary Figure 3 Forces and RhoA distribution evolve with similar kinetics. A) Successive force profiles acquired after finger onset. $t=0$ represent the onset of the finger as visually determined. The profiles at early times are of smaller amplitude and shifted closer to the epithelium. B) Dynamic evolution of the force measured at the tip (coincides with the maximal force) for 3 fingers assessed from 3 independent experiments (one

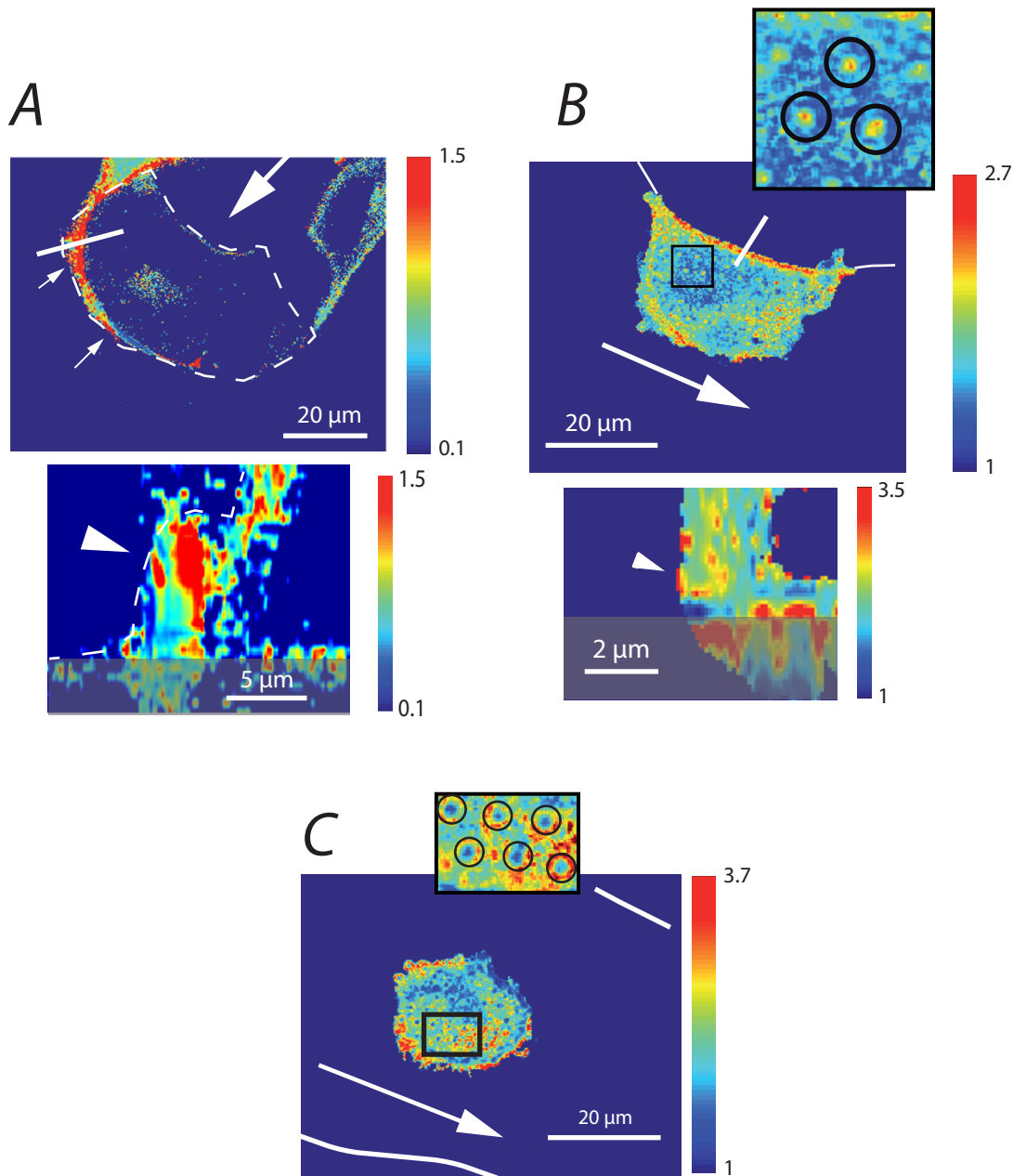
color stands for one finger), the line is an exponential fit of all the data. Error bars are the experimental absolute uncertainty. C) Representative cell becoming a leader within the epithelium (left), at the onset of the finger (center) and when the finger is fully developed (right). The gradient of RhoA activity in the leader cell sets up at similar time scales at the onset of a finger. Representative image. 3 replicates.

A	<i>Control</i>	<i>ROCK Inhibitor (Y27632)²</i>	<i>Myosin inhibitor (Blebbistatin)³</i>	<i>RhoA inhibitor (C3-transferase)⁴</i>	<i>Rac GEF inhibitor (NSC23766)⁵</i>
<i>t₀ + 20 hrs</i>					
<i>Phenotype of fingers and leaders</i>	Well-formed fingers, leader cells	no leader, no finger	short lived leaders (< 2hrs) Short fingers (< 70 μm)	No leader, no finger (locally active protrusions)	Not different from control
<i>Front velocity (μm/h)</i>	11.2 ± 3.6	5.9 ± 1.3	14.6 ± 2.7	3.9 ± 1.1	9.5 ± 1.8
<i>Action on preformed fingers</i>	NA	Suppresses all leaders & fingers	Suppresses most of the fingers	Suppresses fingers	Not different from control



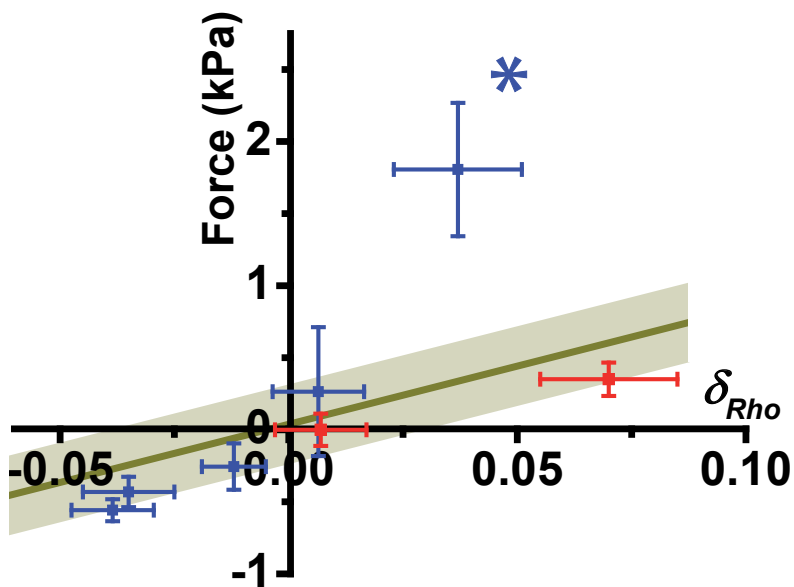
Supplementary Figure 4 Fingers are under RhoA control. **(A)** Use of chemical inhibitors. The drugs were used either at the beginning of the experiments or 4–6 hours after stencil removal to highlight their action on finger formation or on their maintenance. Leaders are identified by their phenotype (larger cells, active ruffling lamellipodium). Bars are 250 μm. n = 6 independent experiments. Errors are SEMs. **(B)** Validation of anti-RhoA siRNAs. Western blots anti-Rac1 and anti-RhoA were performed on lysates of MDCK cells not-transfected or treated with control siRNA, siRhoA#1 or siRhoA#2. Expression levels were normalized towards

GAPDH (not shown) and the no-transfection condition was used as reference. **(C)** Distribution of RhoA differential activity along a finger in presence of C3 Transferase. The Rho inhibitor results in a strong decrease of δ_{Rho} (Blue). This decrease mirrors the response of the force profile in similar RhoA-inhibition conditions (Fig. 4B). Red points are the RhoA differential activity with no RhoA inhibition (from Fig. 5F). Observations were performed after 2hrs incubation of C3 transferase on n = 16 cells spanning 12 well-defined fingers from 2 independent experiments. Error bars are SEMs.



Supplementary Figure 5 Confocal imaging of RhoA activity for cells migrating on a micropillar array. In all the images, the large arrows is within the finger and points to the leader cell. **(A)** Leader cell: the high level of RhoA activity is highlighted by arrows and is colocalized with the lamella. In the xy image (top panel), the cell contour is outlined with a dashed line. This image is taken ~ 4 μm above the tops of the pillars (triangle on the xz section (bottom panel)). The dashed line on the xz section outlines the lamella. **(B)** Enhancement of the activity at the free edge of the finger where it is colocalized with the actin cable. Top panel: xy section; bottom panel xz

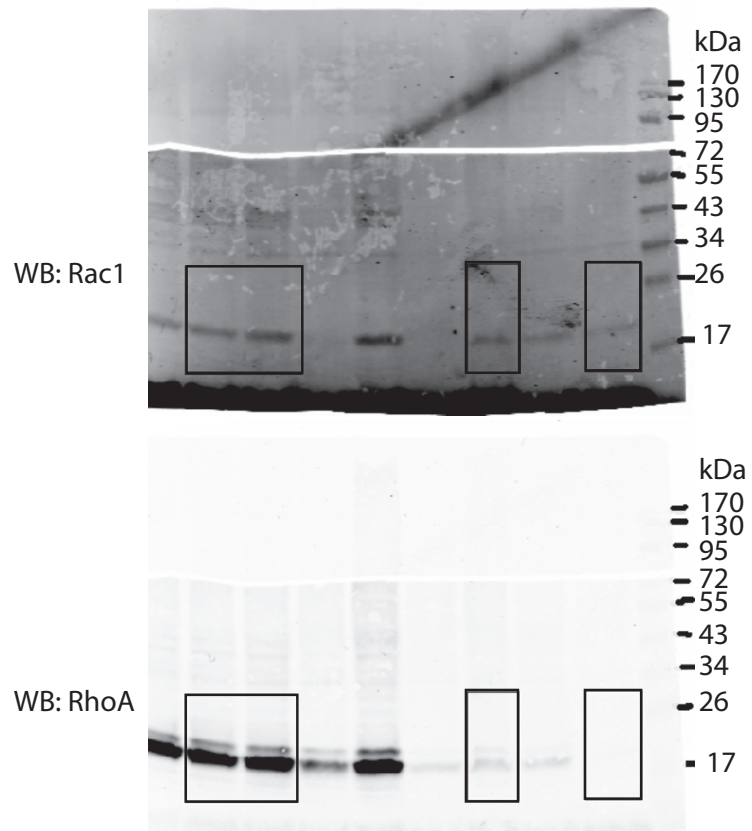
section. In both **(A)** and **(B)** images, the xz section are taken along the white line of the corresponding xy image. The grey box at the bottom represents a volume below the top of the pillars where imaging is not reliable. **(C)** at the basis of the finger, the polarity is very weak (front side and backside activities are comparable). In images **(B)** and **(C)**, the top of the pillars are clearly apparent (insets). Note that image processing was optimized for FRET differences (colour differences), rather than biosensor localization (signal intensity). Representative images. 3–6 replicates from 3 independent experiments.



Supplementary Figure 6 Force-RhoA activity relationship. Force was plotted against d_{Rho} for cells identically positioned in a finger in normalized coordinates. This Figure is the equivalent of Fig. 6B for a normalized “average finger” derived from several independent experiments. Points have been binned according to their position along and across the fingers and average force and Rho activity values within these bins are reported

on this graph. Blue points: longitudinal direction, Red points: transverse direction. The line is the sensitivity as measured in the confocal plane (Fig. 6B). It describes well most of the points with the exception of the leaders (asterisk). Error bars are SEMs. Longitudinal direction: n = 30 cells assessed from 7 experiments. Transverse direction: n = 20 cells assessed from 5 experiments.

SUPPLEMENTARY INFORMATION



Supplementary Figure 7 Uncropped Western Blot with markers of Supplementary Figure 4B.

REFERENCES

1. Saez, A., Buguin, A., Silberzan, P. & Ladoux, B. Is the mechanical activity of epithelial cells controlled by deformations or forces? *Biophys. J.* **89**, L52–4 (2005).
2. Sutton, T. A., Mang, H. E. & Atkinson, S. J. Rho-kinase regulates myosin II activation in MDCK cells during recovery after ATP depletion. *Am. J. Physiol. Physiol.* **281**, F810 (2001).
3. Straight, A. F. et al. Dissecting temporal and spatial control of cytokinesis with a myosin II Inhibitor. *Science* **299**, 1743–7 (2003).
4. Gopalakrishnan, S., Raman, N., Atkinson, S. J. & Marrs, J. A. Rho GTPase signaling regulates tight junction assembly and protects tight junctions during ATP depletion. *Am. J. Physiol. Physiol.* **275**, C798 (1998).
5. Desai, R. a, Gao, L., Raghavan, S., Liu, W. F. & Chen, C. S. Cell polarity triggered by cell-cell adhesion via E-cadherin. *J. Cell Sci.* **122**, 905–11 (2009).

Supplementary Video Legends

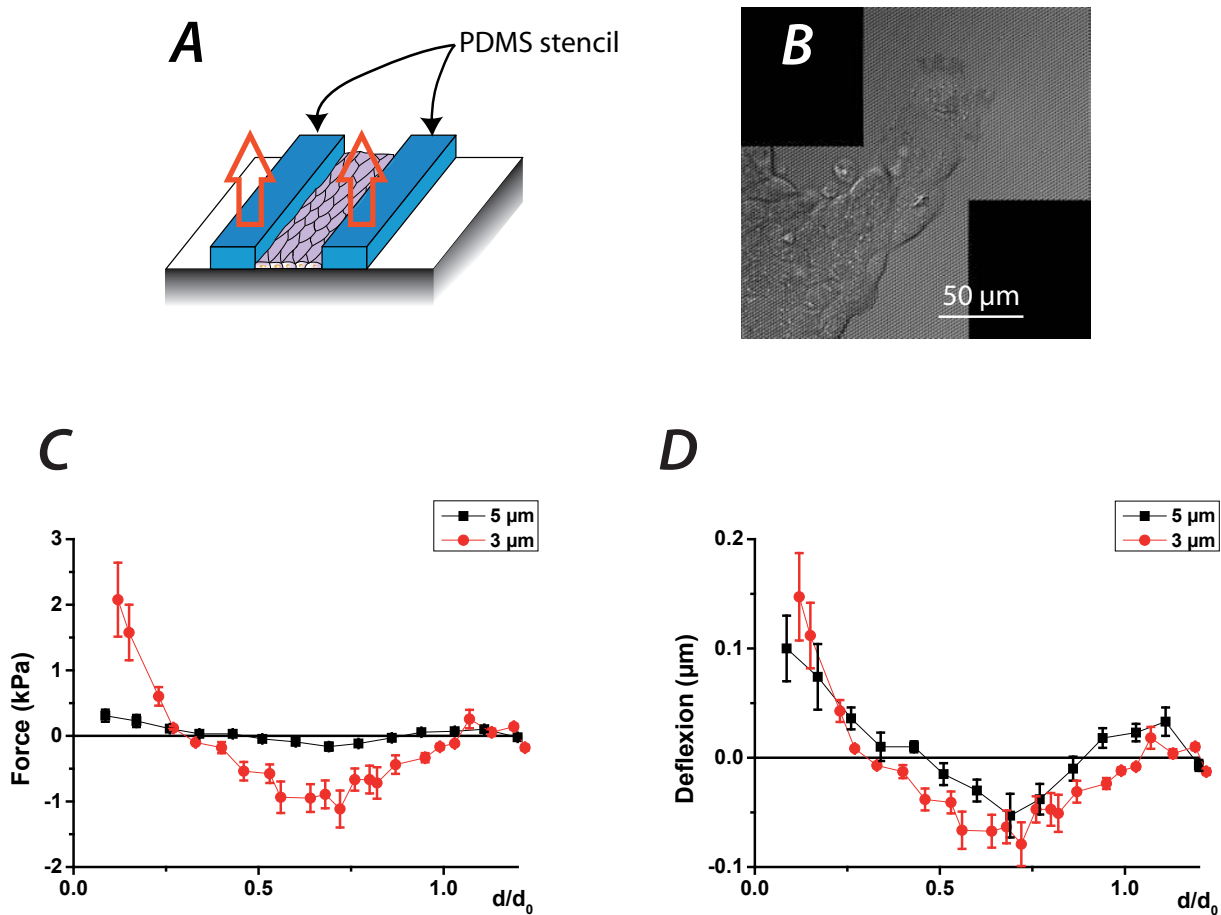
Supplementary Video 1 Retraction of the actin cable after photoablation. The actin-GFP MDCK cells forming a migration finger identical to the wild type cells. Two-photon laser photoablation severed the peripheral actin cable whose retraction indicates that it is under tension. Time interval is 30 s. Scale bar indicates 20 microns.

Supplementary Video 2 Onset of new leader at a weak point of the actin cable. After severing of the peripheral cable (see Supp. Movie 1), a new leader emerges at the exact point of ablation. Time delay is indicated on the right upper corner. Time interval is 15 min. Scale bar indicates 20 micron.

Supplementary Video 3 Distribution of RhoA activity in a leader cell preceding a finger. This cell is transfected with the RhoA biosensor. Note the higher RhoA activity at the front side of the leader compared to the backside.

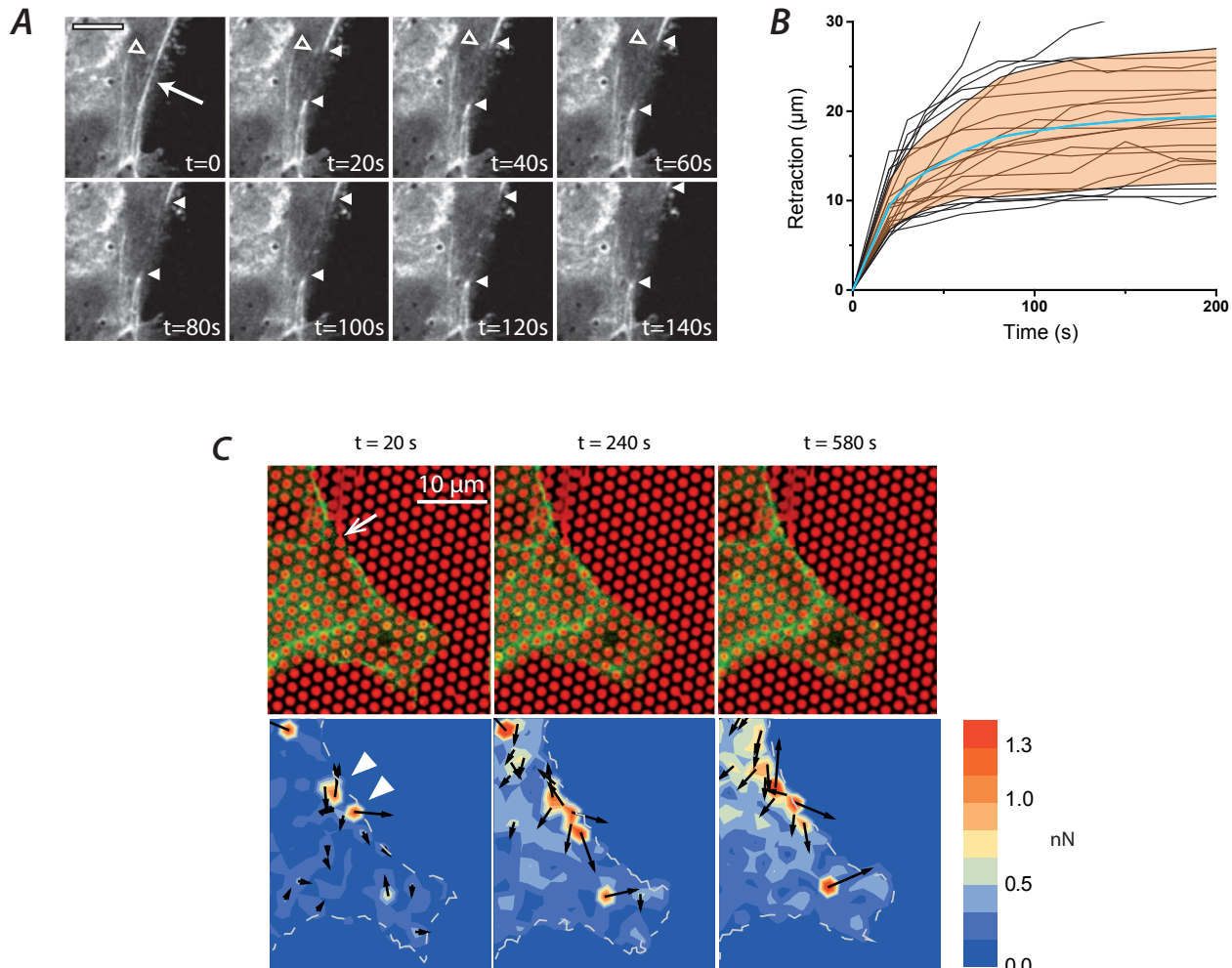
Supplementary Video 4 Distribution of RhoA activity in a finger cell close to the epithelium. This cell is transfected with the RhoA biosensor. Note the higher RhoA activity at the backside of the cell compared to its front side.

Supplementary Video 5 Distribution of Rac1 activity in a leader cell preceding a finger. This cell is transfected with the Rac1 biosensor. Note the higher Rac1 activity at the back side of the leader compared to its front side.



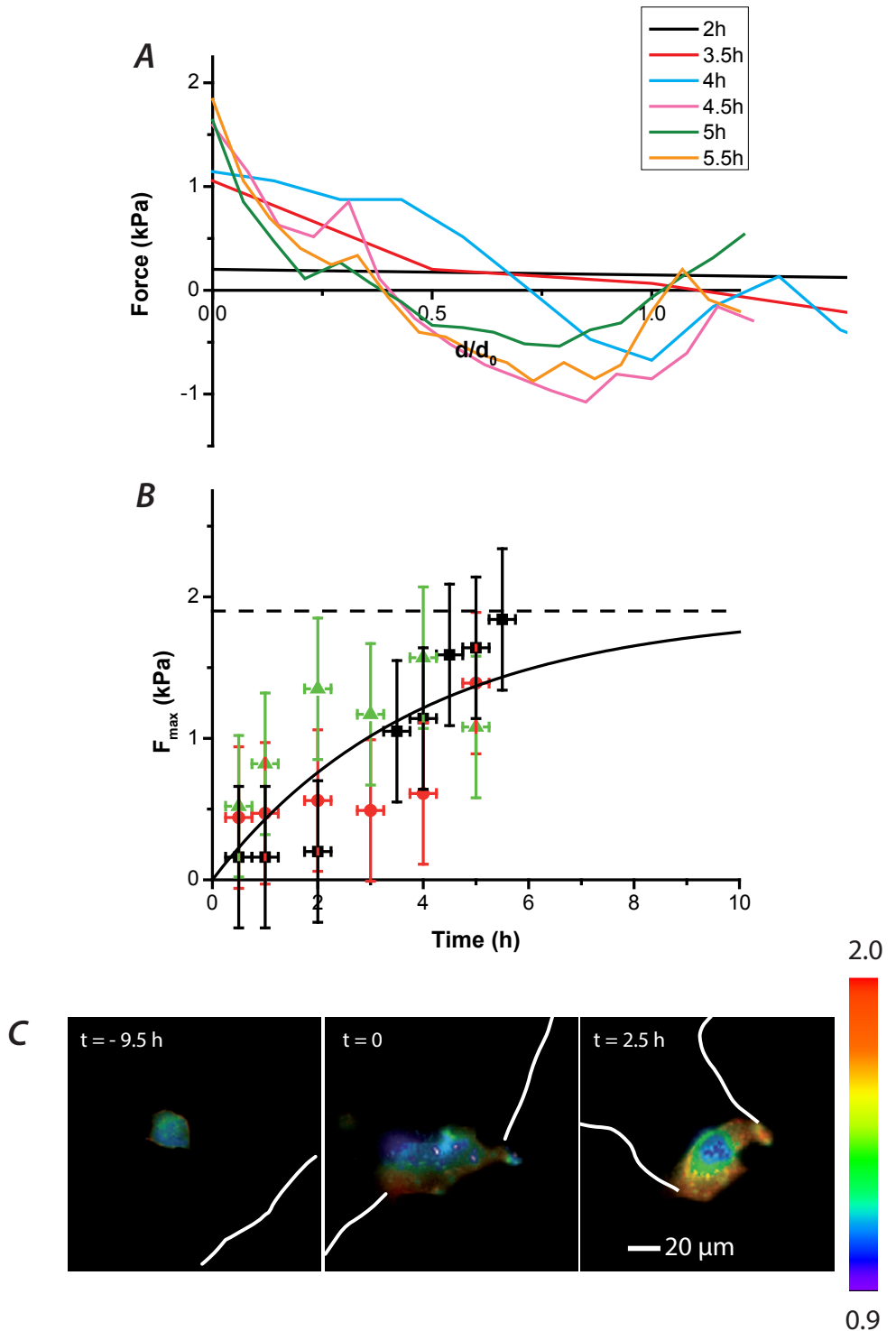
Supplementary Figure 1 Migration fingers respond to the micropillar array rigidity. (A) Experimental set-up. The microstencil is deposited on the surface; cells are then seeded and cultured until confluence in the apertures. Peeling off the stencil triggers cell migration on the free surface. (B) Fingers develop well on a micropillar array. Phase contrast image of the migrating front on a micropillar array. The fingers are clearly identified. They are preceded by a leader cell of a specific phenotype. Representative image, more than 20 replicates. (C-D) Influence of the substrate rigidity on the force profile. (C)

Forces were measured on substrates differing on the height of the pillars and hence on their effective rigidity (see Material and Methods). The absolute forces were very different. (D) In contrast, the deflection of the pillars does not depend on their rigidity (i.e. the forces are proportional to the surface rigidity). 5 μm high pillars correspond to an effective Young Modulus of 1.7 kPa; 3 μm high pillars correspond to an effective Young modulus of 7.8 kPa¹. 5μm-pillars: n = 10 fingers from 3 independent experiments; 3μm-pillars: n = 9 fingers from 3 independent experiments. Error bars are SEMs.



Supplementary Figure 2 The peripheral actin cable is under tension and interacts directly with the substrate (**A**) Image sequence following the severing of the actin-GFP cable by photoablation (scale bar 10 μm). The white arrow indicates the initial ablation. The solid triangles denote the extremities of the retracting cable (see also Supp. Movie 1). Note that small structures next to the cable retract as well (empty triangle), demonstrating that this is a tension driven relaxation. Representative images. More than 20 replicates. (**B**) Distance between the two extremities of the cable as a function of time. The cyan line is the average of the different independent measurements (black curves), yielding a characteristic time of 37 ± 7 s

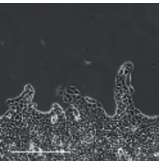
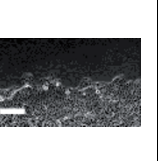
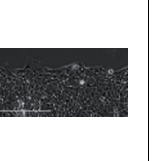
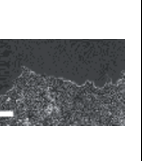
(SD) after a fit by an exponential function. The orange area is the standard deviation over 20 experiments. (**C**) When cut by photoablation (top panel, arrow), not only the forces at the cut relax but also the neighboring pillars situated under the cable. $t=0$ is the time of ablation. Top panel = actin-GFP and pillars – bottom panel = local forces (colours give the intensity and arrows the direction). The white triangles denote the high forces at pillars next to the cut. Note that the relaxation at longer times involves more pillars at a distance from the physical cut which demonstrates the direct interaction of the tensile actin cable with the substrate. Representative image. 20 replicates.

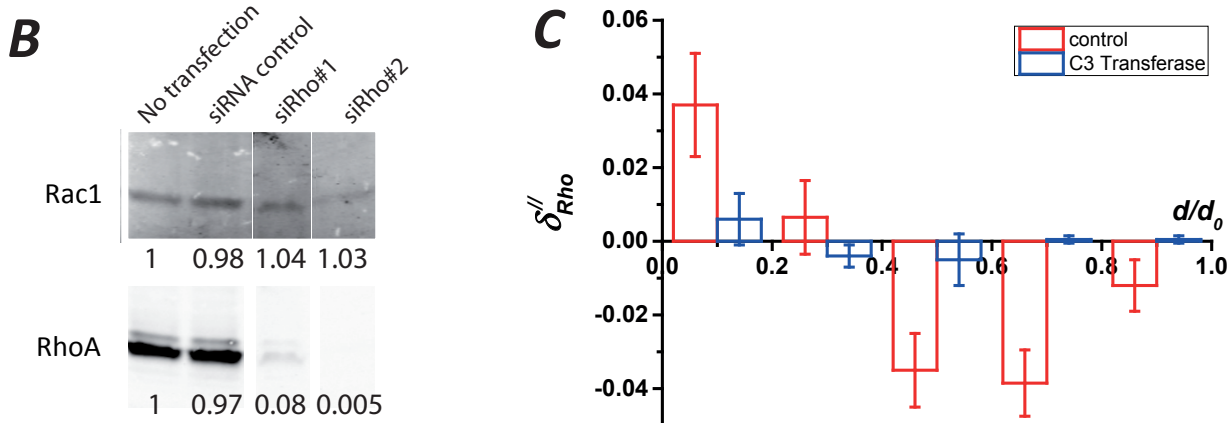


Supplementary Figure 3 Forces and RhoA distribution evolve with similar kinetics. A) Successive force profiles acquired after finger onset. $t=0$ represent the onset of the finger as visually determined. The profiles at early times are of smaller amplitude and shifted closer to the epithelium. B) Dynamic evolution of the force measured at the tip (coincides with the maximal force) for 3 fingers assessed from 3 independent experiments (one

color stands for one finger), the line is an exponential fit of all the data. Error bars are the experimental absolute uncertainty. C) Representative cell becoming a leader within the epithelium (left), at the onset of the finger (center) and when the finger is fully developed (right). The gradient of RhoA activity in the leader cell sets up at similar time scales at the onset of a finger. Representative image. 3 replicates.

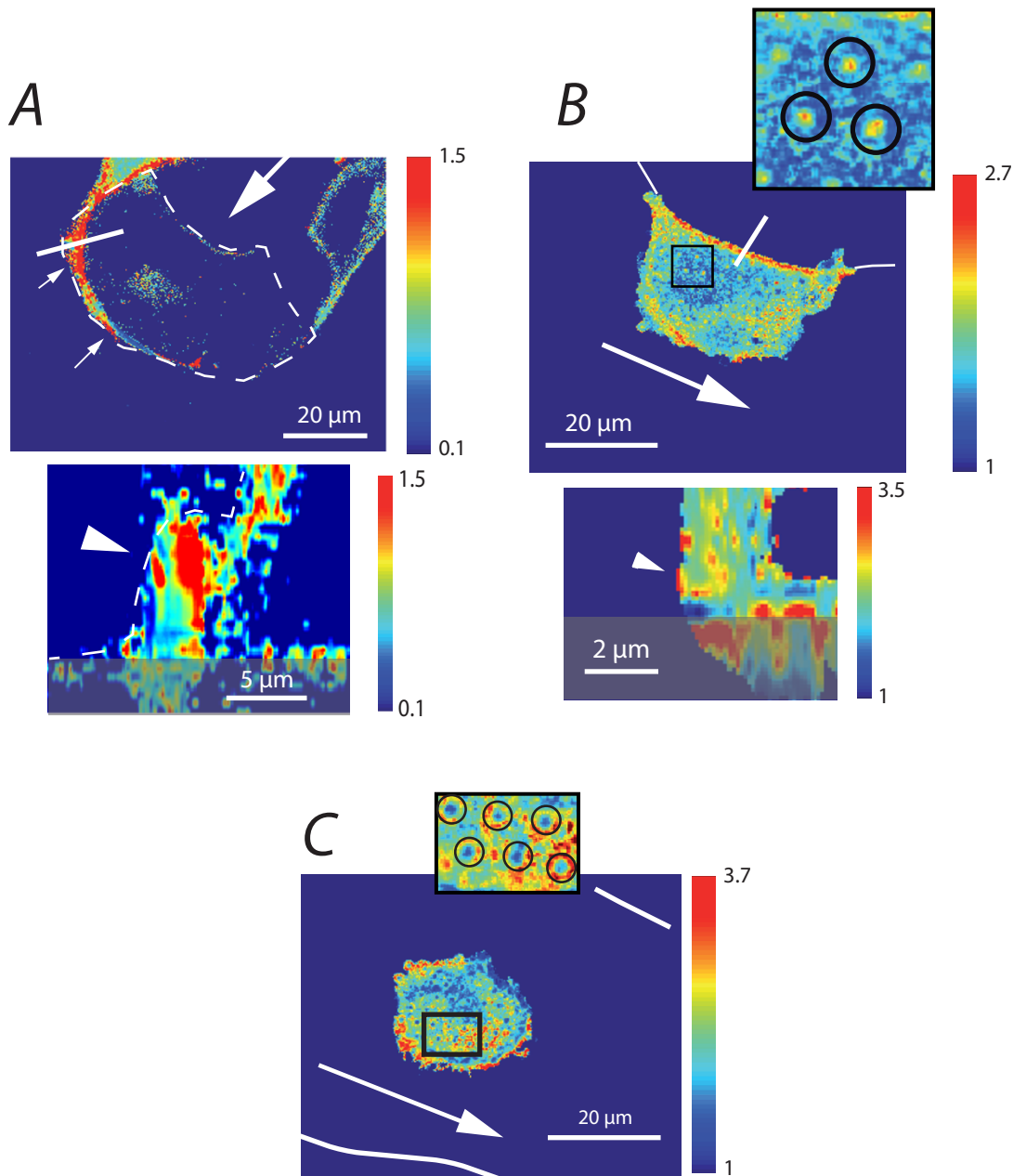
A

	<i>Control</i>	<i>ROCK Inhibitor (Y27632)²</i>	<i>Myosin inhibitor (Blebbistatin)³</i>	<i>RhoA inhibitor (C3-transferase)⁴</i>	<i>Rac GEF inhibitor (NSC23766)⁵</i>
<i>t₀ + 20 hrs</i>					
<i>Phenotype of fingers and leaders</i>	Well-formed fingers, leader cells	no leader, no finger	short lived leaders (< 2hrs) Short fingers (< 70 μm)	No leader, no finger (locally active protrusions)	Not different from control
<i>Front velocity (μm/h)</i>	11.2 ± 3.6	5.9 ± 1.3	14.6 ± 2.7	3.9 ± 1.1	9.5 ± 1.8
<i>Action on preformed fingers</i>	NA	Suppresses all leaders & fingers	Suppresses most of the fingers	Suppresses fingers	Not different from control



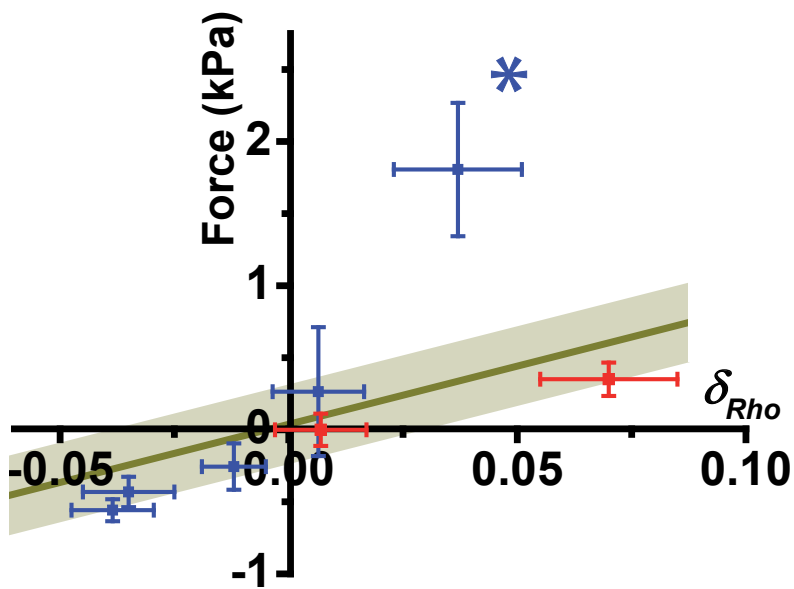
Supplementary Figure 4 Fingers are under RhoA control. **(A)** Use of chemical inhibitors. The drugs were used either at the beginning of the experiments or 4–6 hours after stencil removal to highlight their action on finger formation or on their maintenance. Leaders are identified by their phenotype (larger cells, active ruffling lamellipodium). Bars are 250 μm. n = 6 independent experiments. Errors are SEMs. **(B)** Validation of anti-RhoA siRNAs. Western blots anti-Rac1 and anti-RhoA were performed on lysates of MDCK cells not-transfected or treated with control siRNA, siRhoA#1 or siRhoA#2. Expression levels were normalized towards

GAPDH (not shown) and the no-transfection condition was used as reference. **(C)** Distribution of RhoA differential activity along a finger in presence of C3 Transferase. The Rho inhibitor results in a strong decrease of δ_{Rho}'' (Blue). This decrease mirrors the response of the force profile in similar RhoA-inhibition conditions (Fig. 4B). Red points are the RhoA differential activity with no RhoA inhibition (from Fig. 5F). Observations were performed after 2hrs incubation of C3 transferase on n = 16 cells spanning 12 well-defined fingers from 2 independent experiments. Error bars are SEMs.



Supplementary Figure 5 Confocal imaging of RhoA activity for cells migrating on a micropillar array. In all the images, the large arrows is within the finger and points to the leader cell. **(A)** Leader cell: the high level of RhoA activity is highlighted by arrows and is colocalized with the lamella. In the xy image (top panel), the cell contour is outlined with a dashed line. This image is taken ~4 μm above the tops of the pillars (triangle on the xz section (bottom panel)). The dashed line on the xz section outlines the lamella. **(B)** Enhancement of the activity at the free edge of the finger where it is colocalized with the actin cable. Top panel: xy section; bottom panel xz

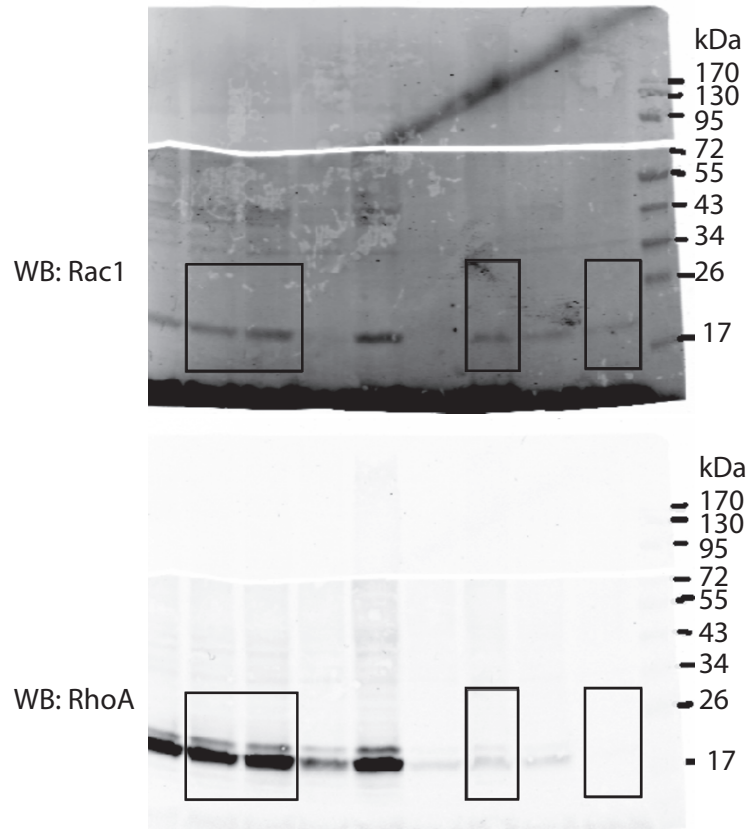
section. In both **(A)** and **(B)** images, the xz section are taken along the white line of the corresponding xy image. The grey box at the bottom represents a volume below the top of the pillars where imaging is not reliable. **(C)** at the basis of the finger, the polarity is very weak (front side and backside activities are comparable). In images **(B)** and **(C)**, the top of the pillars are clearly apparent (insets). Note that image processing was optimized for FRET differences (colour differences), rather than biosensor localization (signal intensity). Representative images. 3–6 replicates from 3 independent experiments.



Supplementary Figure 6 Force-RhoA activity relationship. Force was plotted against d_{Rho} for cells identically positioned in a finger in normalized coordinates. This Figure is the equivalent of Fig. 6B for a normalized “average finger” derived from several independent experiments. Points have been binned according to their position along and across the fingers and average force and Rho activity values within these bins are reported

on this graph. Blue points: longitudinal direction, Red points: transverse direction. The line is the sensitivity as measured in the confocal plane (Fig. 6B). It describes well most of the points with the exception of the leaders (asterisk). Error bars are SEMs. Longitudinal direction: n = 30 cells assessed from 7 experiments. Transverse direction: n = 20 cells assessed from 5 experiments.

SUPPLEMENTARY INFORMATION



Supplementary Figure 7 Uncropped Western Blot with markers of Supplementary Figure 4B.

REFERENCES

1. Saez, A., Buguin, A., Silberzan, P. & Ladoux, B. Is the mechanical activity of epithelial cells controlled by deformations or forces? *Biophys. J.* **89**, L52–4 (2005).
2. Sutton, T. A., Mang, H. E. & Atkinson, S. J. Rho-kinase regulates myosin II activation in MDCK cells during recovery after ATP depletion. *Am. J. Physiol. Physiol.* **281**, F810 (2001).
3. Straight, A. F. et al. Dissecting temporal and spatial control of cytokinesis with a myosin II Inhibitor. *Science* **299**, 1743–7 (2003).
4. Gopalakrishnan, S., Raman, N., Atkinson, S. J. & Marrs, J. A. Rho GTPase signaling regulates tight junction assembly and protects tight junctions during ATP depletion. *Am. J. Physiol. Physiol.* **275**, C798 (1998).
5. Desai, R. a, Gao, L., Raghavan, S., Liu, W. F. & Chen, C. S. Cell polarity triggered by cell-cell adhesion via E-cadherin. *J. Cell Sci.* **122**, 905–11 (2009).

Supplementary Video Legends

Supplementary Video 1 Retraction of the actin cable after photoablation. The actin-GFP MDCK cells forming a migration finger identical to the wild type cells. Two-photon laser photoablation severed the peripheral actin cable whose retraction indicates that it is under tension. Time interval is 30 s. Scale bar indicates 20 microns.

Supplementary Video 2 Onset of new leader at a weak point of the actin cable. After severing of the peripheral cable (see Supp. Movie 1), a new leader emerges at the exact point of ablation. Time delay is indicated on the right upper corner. Time interval is 15 min. Scale bar indicates 20 micron.

Supplementary Video 3 Distribution of RhoA activity in a leader cell preceding a finger. This cell is transfected with the RhoA biosensor. Note the higher RhoA activity at the front side of the leader compared to the backside.

Supplementary Video 4 Distribution of RhoA activity in a finger cell close to the epithelium. This cell is transfected with the RhoA biosensor. Note the higher RhoA activity at the backside of the cell compared to its front side.

Supplementary Video 5 Distribution of Rac1 activity in a leader cell preceding a finger. This cell is transfected with the Rac1 biosensor. Note the higher Rac1 activity at the back side of the leader compared to its front side.

Interplay of RhoA and mechanical forces in collective cell migration driven by leader cells

M. Reay, M. C. Parrini, O. Cochet-Escartin, B. Ladoux, A. Buguin, S. Coscoy, F. Amblard, J. Camonis and P. Silberzan

Nat. Cell Biol. **16**, 217–223 (2014); published online 23 February 2014; corrected after print 26 February 2014

In the version of this Article originally published there were some errors:

The second citation of reference 1 in the first sentence of the main text should have been of reference 2 ('...or by the release of a physical barrier²...').

The present addresses of B. Ladoux were missing the area codes ('Paris F75205' and '117411 Singapore').

The caption of Fig. 1d–f should have read: '(d,e) Force profiles in the parallel and perpendicular directions resulting from averaging forces for 22 and 12 fingers from 15 and 10 independent experiments respectively. The thick red line is the average profile, the coloured area represents the standard deviation. (f) Schematic representation of the direction of the forces: the leader cell exerts a stable traction longitudinal force whereas the forces in the fingers are highly dynamic and can be positive or negative (red arrows). The side edges exert a centripetal force (green arrows). Fingers were composed of typically 30 cells.'

In the first sentence of the second paragraph under the heading 'Migration fingers are mechanical global entities', the figure citation should have read 'Fig. 1d,e'.

The first part of the caption of Fig. 3c should have read: '(c) The flow lines that show the direction...'

The citation of 'Supplementary Fig. 4C,B' in the first paragraph under the heading 'The supracellular distribution of RhoA activity mirrors the cartography of forces' should have read 'Fig. 4b and Supplementary Fig. 4C'.

The page ranges for refs 17, 28, 44, 46 were missing; they are 15895–15900, 1313–1323, 6582–6591 and 1836–1843, respectively.

All these errors have been corrected in the online versions of the Article.